2016

A Geochronological and Stratigraphic Reconstruction of the Middle Barataria Bay Receiving Basin

Joseph Ethan Thomas Hughes
Louisiana State University and Agricultural and Mechanical College

A GEOCHRONOLOGICAL AND STRATIGRAPHIC RECONSTRUCTION OF THE MIDDLE BARATARIA BAY RECEIVING BASIN

A Thesis

Submitted to the Graduate Faculty of the
Louisiana State University and
College of Science
in partial fulfillment of the
requirements for the degree of
Master of Science

In

The Department of Geology and Geophysics

by
Joseph Ethan Thomas Hughes
B.S., Millsaps College, 2013
December 2016

Acknowledgments

My advising professor, Dr. Samuel J. Bentley, and the assistance of his entire student lab. In particular, the efforts of Crawford White, Edwin J. Bomer, and Frances R. Crawford.

The LSU Coastal Studies Institute, for providing the manpower and resources to make this work possible.

Dr. Carol Wicks and Dr. Kehui Xui, for serving on the project committee, and contributing to the quality of this study.

The Coastal Protection and Restoration Authority, via the Water Institute of the Gulf, for providing the necessary funding for this research.

The Louisiana Department of Wildlife and Fisheries alongside various local landowners, for permitting samples to be collected from the project study area.

Table of Contents

Abstract

Barataria Bay, one of the largest receiving basins for the Mississippi deltaic complex, is the location of a proposed river-sediment diversion for delta restoration. In order to determine how the sediment in the receiving-basin may respond to diversion flows, twenty-five sediment vibracores were collected from a 115 km^2 study area located near Myrtle Grove and Bayou Dupont, southeast of New Orleans, LA. These cores were subject to multiple tests, including gamma bulk density scans, grain size analysis, and loss-on-ignition, in order to identify the lithology and stratigraphy. In addition, ^{137}Cs and ^{14}C dating techniques were employed in order to construct a geochronology. A subdelta lithofacies succession was identified and stratigraphically correlated across the basin, indicating more than one subdelta cycle in the sediment record. Geochronology suggests at least one St. Bernard subdelta entered dormancy within the range of 2130 to 2770 ± 30 ^{14}C years BP, a period that lasted a minimum of 860 ± 30 ^{14}C years, followed by Plaquemines-Belize subdelta progradation that ceased between 280 to 870 ± 30 ^{14}C years BP. The presence of channel sands and surviving St. Bernard age peats in the near-surface suggests resistance to compression and subsidence at depths greater than 2 m, providing a viable foundation for stable platform development from the mineral sediment nourishment of a large-scale diversion.

Chapter 1. Introduction

On the lower Mississippi River Delta, ongoing loss of wetlands due to environmental and anthropogenic activity continues to be a challenge for coastal restoration efforts in Louisiana, USA. Factors driving wetland loss include artificial levees, an extensive dam network, and the natural forces of ongoing sea-level rise and subsidence (Blum and Roberts, 2012). Barataria Bay, one of the largest receiving basins for the Mississippi deltaic complex, is a major site for a proposed river-sediment diversion (LACPRA, 2012). The restoration objective is to re-direct the Mississippi River's sediment load back into the marshland in order to build new land and sustain existing wetlands (Allison and Meselhe, 2010). In order for this plan to succeed, the conservation potential of the new sediment deposited in the wetlands must outweigh the quantity of sediment scoured by the increased influx, requiring a qualified geological understanding of the designated receiving basins, with particular value placed on sediments that can withstand the shear stress of incoming material.

To better understand the geology and stratigraphy of the receiving basin, twenty-five sediment vibracores were collected from a 115 km^2 study area located near Myrtle Grove and Bayou Dupont. The goal of this work is to map basin-wide stratigraphy, identify the existing lithofacies, develop historical depositional age models, and reconstruct a geochronological history for the study area and the associated delta lobes. Stratigraphic analysis formed the core of interpretation, with the primary tools of investigation being multi-sensor core logging, grain size analysis, loss-on-ignition testing, and radiometric carbon dating. These geochronological results contribute new age

constraints to the area south of New Orleans, significantly affecting the interpreted history of the Mississippi paleo-delta lobes.

1.1. Study Area: Barataria Bay

Barataria Bay is located south of New Orleans, is geologically part of the Barataria interdistributary basin, and is influenced by the Plaquemines-Belize, St. Bernard, and LaFourche deltaic complexes during the past 4000 years (Fitzgerald et al., 2004). The study area, referred to as "Middle Barataria Basin" (MBA, Figure 1), is located in the northeastern portion of the basin; its recent depositional development is probably most closely tied to the St. Bernard, LaFourche, and Plaquemines delta lobes (Blum and Roberts, 2012). In particular, the streams of Bayou Barataria were active during the St. Bernard phase of delta building in the alluvial valley (Fisk, 1944.)

While there have been several studies attempting to date the different delta lobes of the Mississippi (discussed in Bentley et al., 2015), Tornqvist et al. (1996) presented the most recent authoritative chronology of the delta. Their model was developed by sampling the top of peat beds underneath clay-rich overbank deposits located at the conjunction of the trunk channels of the previously mentioned three delta lobes (St. Bernard, LaFourche, and Plaquemines). The ^{14}C ages of these samples act as the basis for an estimation of the inception of fluvial activity, whereas additional dates from the bottom of the organics-dominated beds above document cessation of the most active fluvial processes. The results of Tornqvist et al. (1996) introduced a revised St. Bernard origin of activity at a weighted average of 3569 ± 24 ^{14}C years B.P.,

whereas onset of the LaFourche and Plaquemines progradation phases are estimated at 1491 ± 13 and 1322 ± 22 ^{14}C years B.P., respectively. In particular, these results indicate a much younger age for the LaFourche delta lobe relative to the work of Roberts (1997). This revised chronology is used as the basis for chronological interpretations herein for the Middle Barataria Basin.

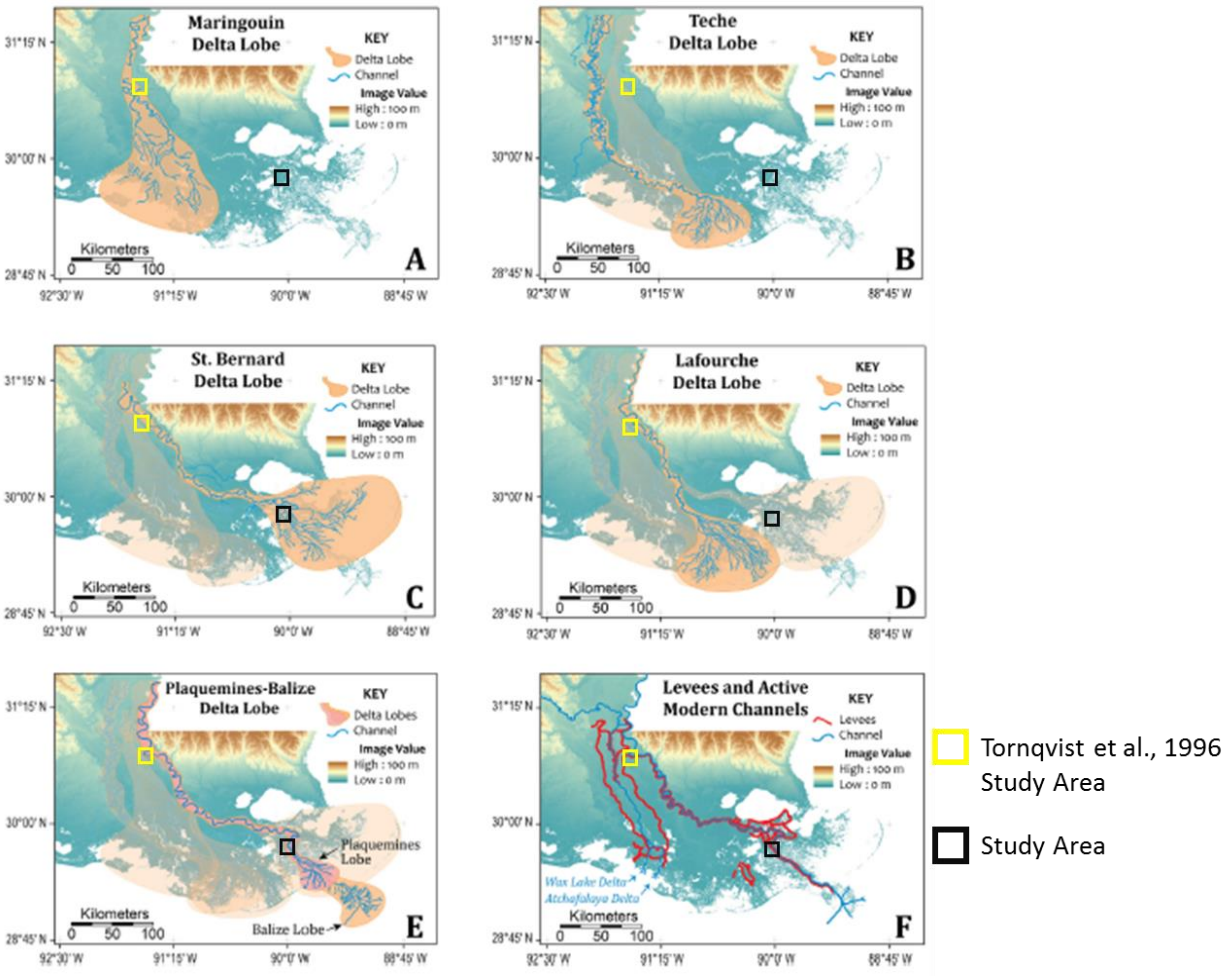

Figure 1. The study area transposed upon paleo-delta lobe complexes of the Mississippi Delta. Also shown is the study area for Tornqvist et al., 1996, the most recent radiocarbon dating results for the Mississippi delta. (Modified from Bentley, 2015).

Interdistributary bays have been defined as the "areas between deltaic distributaries," and thus include a basin such as Barataria (Coleman, 1988). These bays are morphologically defined by crevasse-splay sands, discrete channels, and natural levees, while their shallow water bodies vary from marine, brackish, to fresh (Coleman, 1988). They are nourished with sediment and nutrients predominantly by flooding from the trunk channel, and thus rely on this nourishment for longevity (Coleman, 1988). Without mineral sediment, the extensive areas of vegetation act as the main sediment contributors with the organic sediment production leading to the thick peat layers that characterize marshland (Elliott, 1974).

The basin is notably sediment starved due to the manmade levee system of the Mississippi's main channel and human closure of Bayou Lafourche, which further reduced fluvial sediment supply to the basin after Mississippi River's course altered from the LaFourche Delta depocenters to the present modern fluvial axis (Bentley et al., 2015). Storm deposits are the only substantial nourishment, aside from man-made diversions (Sasser et al., 1986). The wetland's surficial peaty soils are often susceptible to marsh front erosion and storm-related scour (Fitzgerald et al., 2007). Relative sea-level rise in the bay (~0.94 cm/yr) is among the highest in the continental United States (Fitzgerald et al., 2007). Around 16.9 km^2/yr of wetlands were lost in the area from 1935-2000 (Fitzgerald et al., 2007) making the interdistributary basin a prime example of the prevalent land loss that currently plagues the Mississippi Delta.

1.2. Controls on Delta Morphodynamics

Deltas are governed by a complex interplay of physical, biological, and geochemical processes that guide their evolution, structure, and extent (Wright and Nittrouer, 1995; Paola et al., 2011). They are comprised of linked depositional environments: topset, foreset, and bottomset regions. In the case of the Mississippi Delta, the topset is the low-gradient riverine portion of the upper delta, characterized by wetland and overbank depositional processes, as well as sediment bypass via channel flow (Coleman, 1988). Also for the Mississippi, the foreset begins at the shoreline with a significantly increased gradient, and is characterized by basinward progradation of distributary levees, distributary-mouth bars, and a muddy apron in deeper water, laterally bounded by interdistributary bays. This complex of interfingering depositional environments produces the complex 3-dimensional clinoformal morphology of the river-dominated Mississippi River Delta (Coleman, 1988). The bottomset is comprised of the finest sediments deposited beneath the river plume as it expands basinward over the ambient waters of the receiving basin (Wright and Nittrouer, 1995). The wetland ecosystems of Barataria Bay are situated in the topset, where the foreset transports and stores the sediment delivered via the river system. The bulk of this sediment is transported downslope or along the shoreline, it is occasionally delivered back to the topset through the transport processes of storms and tides (Paola et al., 2011).

River deltas, in their natural state, are remarkably resilient to the drowning effects of rising sea level rise. Given sufficient sediment supply from inland, a delta is capable of aggrading in response to the rise of relative sea level (RSL) (Paola et al.,

2011). Thus, one can see both the inherent risk of a reduced sediment load due to anthropogenic forcing, and the baseline theory for how sediment diversions could preserve the Mississippi Delta in the wake of RSL rise (Paola et al, 2011).

The pre-existing stratigraphy of a proposed diversion-receiving basin also comprises an important control on land development. Peat-based strata are extremely susceptible to erosion and compaction; mud-rich, then sand-rich sediments of successively lower initial water content tend to compact less over time and withstand greater amounts of shear stress (Tornqvist et al., 2008). As all sediment types age and are compacted, the potential for further future compaction diminishes (Tornqvist et al., 2008), implying that older deltaic sediments may make more stable foundations for land-building. As well, more consolidated sediments will tend to have greater resistance to erosion (Xu et al., 2016), which is an important consideration for resistance of existing wetlands to erosion from diversion flows.

The depositional environment of the interdistributary basin lends itself to crevasse-splays from the trunk channel, and possibly even the formation of subdelta lobes (Wells and Coleman, 1987). A crevasse-splay is formed when the water from the trunk channel breaks through its natural levee (usually on the outside curve of a meander), depositing sediment on its floodplain as the water loses energy (and thus, sediment load capacity) (Davis, 2000). A subdelta may develop when the crevasse channel remains an open distributary for years to decades, rather than being closed by natural processes within a few years (Wells and Coleman, 1987.) The associated lithofacies succession in the sedimentary record for subdelta growth and decline is

interbedded sands and silts during the high energy active building phase, fine clays distally deposited during regression, and peat from organic sediment-dominated dormancy (Wells and Coleman, 1987).

Crevasse-splay events may be the first stages of major avulsions, the process that has caused the Mississippi River to switch delta lobes several times in the past (Bentley et al., 2015). Splays are also the basis of the formation of a subdelta lobe, a cyclical phenomenon that lasts 100-200 years and is responsible for the majority of land construction along the modern Bird's Foot delta flanks, such as Cubit's Gap (Figure 2). While crevasse splays are interpreted to cover only a few km^2, with a thickness < 5 m, subdeltas can be approximately 300 km^2 and up to 10 m thick (Roberts, 1997). After the initial break, the subdelta can enlarge via successive flooding, before reaching peak maximum discharge (and deposition) before waning until it is entirely inactive. The compaction and dewatering of the subdelta post-abandonment typically leads to brackish water inundating the basin (reverting to an open-bay environment), the subsequent infilling completing the cycle. Thus, "the subdelta is a scaled down version of a major delta lobe, both in space and time, and can be used as a model for larger-scale deltaic processes" (Wells and Coleman, 1987).

Figure 2. Sequential development of the Cubit's Gap subdelta, constructed from Coast and Geodetic Survey and U.S. Geological Survey charts (Wells, 1987).

Chapter 2. Methodology

The twenty-five vibracores were collected from Middle Barataria Bay (Figure 3), along with piston cores at most locations, using airboats for marsh traversal. The locations were selected in order to encompass a broad region of the receiving basin (> 100 km^2), and also sample the range of depositional environments. The piston corer is composed of a butylene liner (7.2 cm internal diameter), and is intended for short cores (around a meter in length) with minimum compaction. Vibracores are considerably longer, employing an aluminum core barrel 6.5 m long, with a 7.5 cm internal diameter. They are attached to a cement vibrator, the source of their characteristic name and the means by which they penetrate the earth by liquefying the surrounding sediment. While vibracores allow deep penetration, the vibration can cause compaction – thus the need for an additional piston core, which can provide a look at the near-surface strata un-compacted.

After collections, cores were returned to the lab and logged using a Geotek Multi-Sensor Core Logger (MSCL) for gamma density readings at 1 cm intervals. Subsequently, they were split in half length-wise, with the two halves separated into the working sample (used to conduct tests) and the archive sample (kept for a duration to be referenced, and photographed using high resolution imagery). The high resolution imagery was performed using an additional Geotek MSCL, and the cores were kept in refrigerators to preserve their original states, at 4° C.

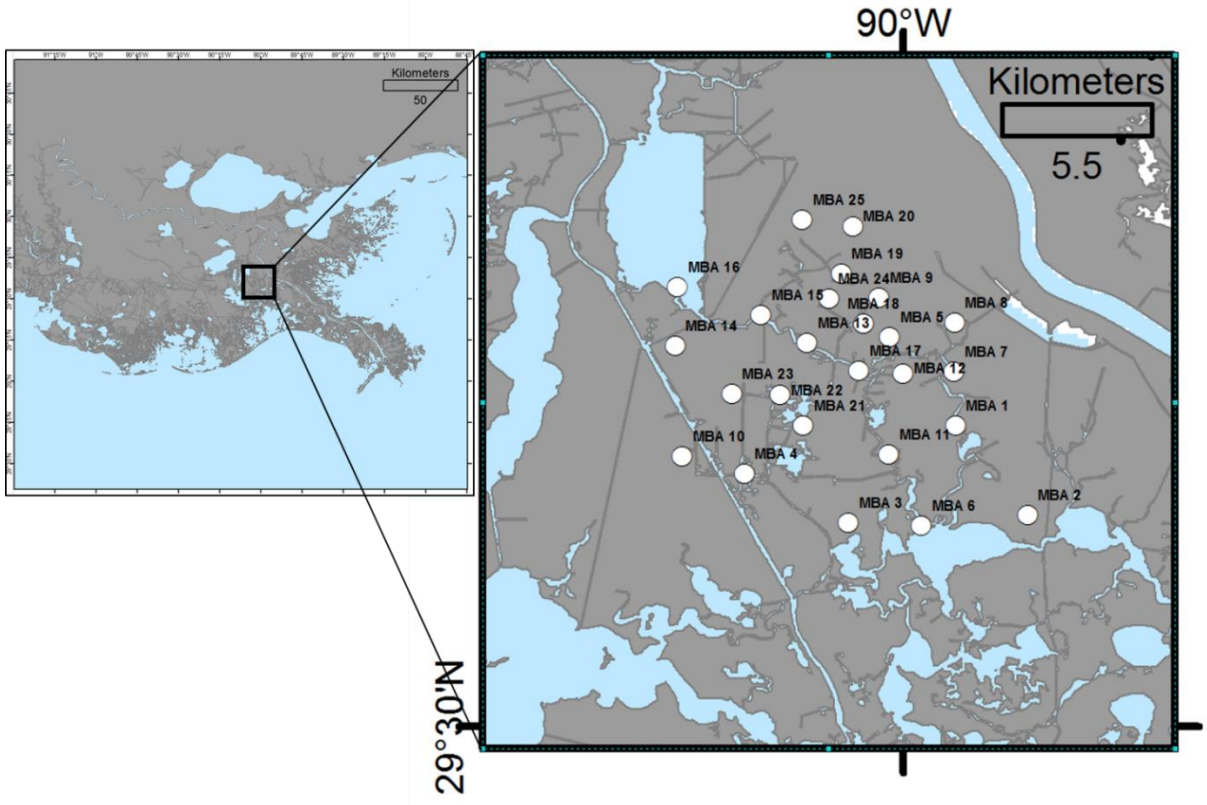

Figure 3. Field sites of the cores collected from Middle Barataria Bay, along the Louisiana Gulf Coast.

Granulometry was performed by taking sediment samples at 25 to 50 cm intervals, adding 5 ml of NaH_2PO_4 (0.05%), and sieving the suspension through an 850 µm sieve in order to remove any large organic particles. Next, 5 ml of H_2O_2 (30%) was added to the sample, which was placed in a hot bath for six hours at 60°C in order to digest any remaining organic material. The sediment that remained was combined with 40 ml 0.05% NaH_2PO_4 before being dispersed in a Beckman Coulter LS13-320 laser diffraction particle size analyzer, which determined the relative grain size abundance. A total of 300 such tests were performed on the collected vibracores.

Loss-on-ignition (LOI) testing involved taking sediment samples every 25 cm and heating them for 72 hours in drying ovens at 60°C, with the sample weight recorded

both before and after the dehydration. The newly dehydrated sediment was thoroughly ground via a mortar and pestle, then combusted for two hours at 550°C. This process ignites all organic material, leaving only mineral content behind (Heiri et al., 2001). A sum of 500 such tests was performed throughout the collected vibracores, with some extra sampled intervals at shallow depths.

An additional tool for dating recent sediment deposition in relation to chronostratigraphy is ^{137}Cs concentrations. Due to its status as a byproduct of nuclear testing beginning in 1953, and reaching an apex in global dispersal in 1963, detectable and peak ^{137}Cs activity in sediment can be used as marker beds for geochronology (Richie et al, 1990). Three piston cores (MBA 08, 17, and 22) were sampled at ten cm intervals for ^{137}Cs activity, including subsamples when necessary. They were dried and ground by means of the same standards set for LOI testing, before being sealed into petri dishes. These samples were then kept for 24-hour activity counting in a single, consistent gamma detector. Activity of ^{137}Cs could be deduced by means of counting the ^{137}Cs peaks relevant to the aforementioned dates. The relevant activities could then be converted to a sediment accumulation rate S using the following formula:

$$S = (z_{max})/(T - 1954) \qquad \text{Eq. 1}$$

with a maximum ^{137}Cs penetration depth of z_{max} (cm), and the year of sample collection T (Nittrouer et al., 1983).

Finally, twelve samples were taken from selected cores, and sent to Beta Analytics, LLC, for ^{14}C dating on plant and bulk sediment material to help with the geochronological reconstruction. The two bulk sediment results produced carbon ages

that did not reflect the depositional age of the material, and were thus not used for geochronological reconstruction. The other ten plant material samples were extracted from the peat facies present in the cores, both at the surface and subjacent at depth, and were sieved at 180 microns to separate sediment and decayed plant remains. These remains were treated at Beta laboratories in order to remove carbonate and mobile humic acids.

Given the degraded nature of the plant remains, there exists a small chance of the dated sediments having been contaminated by invasive roots from the overlying sediment, or of the material being redeposited and consisting of multiple carbon sources originating from different ages of deposition. Because the atmospheric production rate of ^{14}C is not a historical constant, calibration curves have been created using the calendar age of tree rings plotted against their tested radiocarbon age (Talma and Vogel, 1993). The calibration of these ^{14}C samples dates was accomplished using the INTCAL 2013 database in order to determine calendar age, and corrected for total fractionation effects (Reimer et al., 2013). In any circumstance where the produced standard deviations were lower than ± 30 years, the standard deviation has been rounded up to ± 30 in favor of a conservative estimate.

Chapter 3. Results

3.1. Bulk Density

The locations and dimensions of the collected sediment cores are given in Table 1. Bulk gamma density results demonstrate consistent trends of increasing density with depth, including certain recurring modes. Representative density profiles (Figure 4) demonstrate the general downward increase in density, along with small-scale variability that includes saw-tooth patterns over cm-dm scales, as well as thicker zones of more uniform density. The results demonstrate three primary modes of bulk density: ~1-1.35 g/cc, ~1.5-1.75 g/cc, and ~1.75-2.2 g/cc. Transitions between these modes can be observed basin-wide, with some presenting a simple succession (Figure 4, MBA 10) and others presenting repeated modes in a single sequence (Figure 4, MBA 08 and 17).

Table 1. Complete list of sediment cores included in this study. *Exposed core is the amount of tubing that did not penetrate the ground during collection.

Core Name	Latitude	Longitude	Exposed Core* (m)	Hole Depth (m)	Water Depth (m)	Core Length (m)	Non-recovery (m)
MBA 1	29°35'55.80"N	89°58'58.26"W	1.69	4.41	0.20	3.67	0.74
MBA 2	29°34'10.02"N	89°57'33.00"W	0.36	5.74	0.41	5.00	0.74
MBA 3	29°34'0.78"N	90° 1'5.58"W	0.36	5.74	N/A	4.83	0.91
MBA 4	29°34'58.98"N	90° 3'9.36"W	0.39	5.71	N/A	3.99	1.72
MBA 5	29°37'40.86"N	90° 0'16.68"W	0.38	5.72	N/A	4.23	1.49
MBA 6	29°33'57.96"N	89°59'38.76"W	0.55	5.55	N/A	4.35	1.20
MBA 7	29°37'0.00"N	89°59'0.00"W	0.58	5.52	0.75	4.23	1.29
MBA 8	29°37'58.86"N	89°58'59.52"W	0.33	5.77	N/A	3.84	1.93
MBA 9	29°38'28.50"N	90° 0'28.98"W	1.12	4.98	0.70	4.38	0.60
MBA 10	29°35'19.56"N	90° 4'22.74"W	0.53	5.57	N/A	4.49	1.08
MBA 11	29°35'22.62"N	90° 0'17.52"W	0.56	5.54	0.17	3.33	2.21
MBA 12	29°36'58.20"N	90° 0'0.72"W	0.39	5.71	N/A	2.95	2.76
MBA 13	29°37'34.20"N	90° 1'54.90"W	0.37	5.73	N/A	4.01	1.72
MBA 14	29°37'30.84"N	90° 4'31.50"W	0.37	5.73	N/A	3.23	2.50
MBA 15	29°38'7.92"N	90° 2'49.08"W	0.53	5.57	N/A	3.93	1.64
MBA 16	29°38'40.62"N	90° 4'28.80"W	2.29	7.71	1.49	4.87	2.84
MBA 17	29°37'1.26"N	90° 0'52.74"W	1.15	4.95	N/A	3.61	1.34
MBA 18	29°37'57.48"N	90° 0'47.46"W	0.37	5.73	N/A	3.42	2.31
MBA 19	29°38'56.40"N	90° 1'14.28"W	0.35	5.75	N/A	4.31	1.44
MBA 20	29°39'52.32"N	90° 1'0.60"W	0.34	5.76	N/A	4.92	0.84
MBA 21	29°35'56.34"N	90° 1'58.98"W	0.38	5.72	N/A	2.10	3.62
MBA 22	29°36'32.40"N	90° 2'26.76"W	0.45	5.65	N/A	3.91	1.74
MBA 23	29°36'34.26"N	90° 3'24.18"W	3.30	2.80	0.87	2.63	0.17
MBA 24	29°38'27.06"N	90° 1'28.50"W	0.51	5.59	N/A	4.00	1.59
MBA 25	29°40'0.42"N	90° 2'0.84"W	0.33	5.77	N/A	4.50	1.27

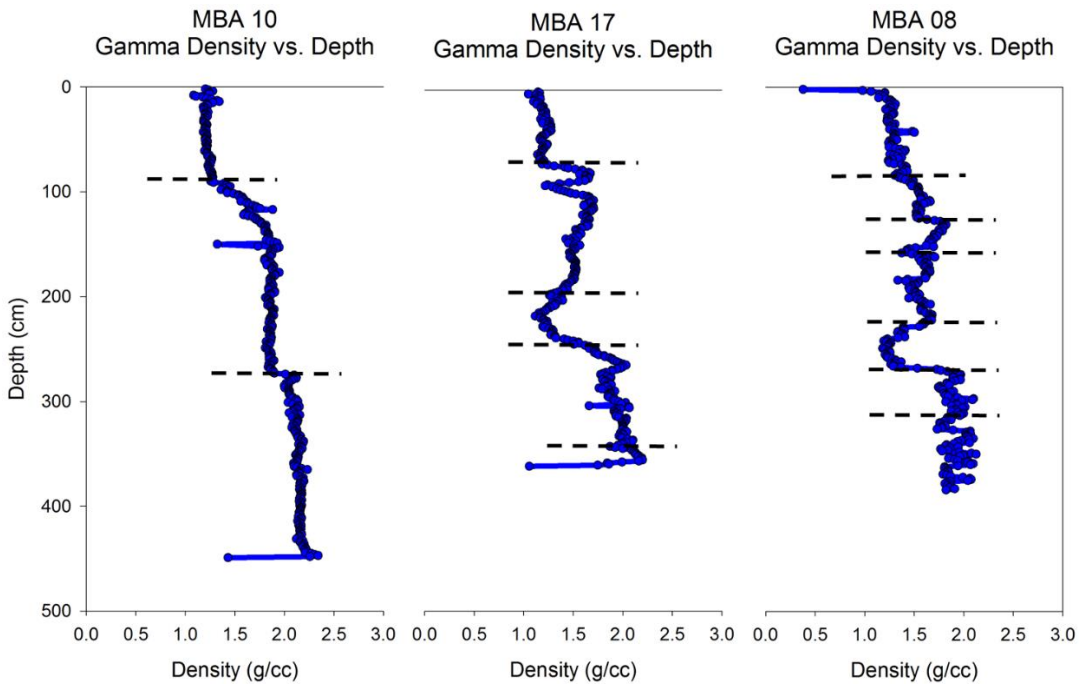

Figure 4. Bulk density at depth for sediment cores MBA 08, 17, and 10. Major transitions of average density occur in each core, denoted by dashed lines. The principal densities present in both these three cores and the basin as a whole are ~1-1.35 g/cc, ~1.5-1.75 g/cc, and ~1.75-2.2 g/cc.

3.2. Granulometry

A summary plot of grain-size volume frequency distribution for the basin can demonstrate the four primary modes (Figure 5). The coarsest fraction is likely to be either shell debris or undigested organics (residual from the digestion process). The other modes (clay and/or fine silt at ~5 microns, fine to very fine sands at ~65-100 microns, and medium sands at ~400-500 microns) are correlative to the stratigraphic transitions seen in the individual physical properties of the cores and the gamma density test results (Figure 4) and grain-size profiles of cores (Figure 6).

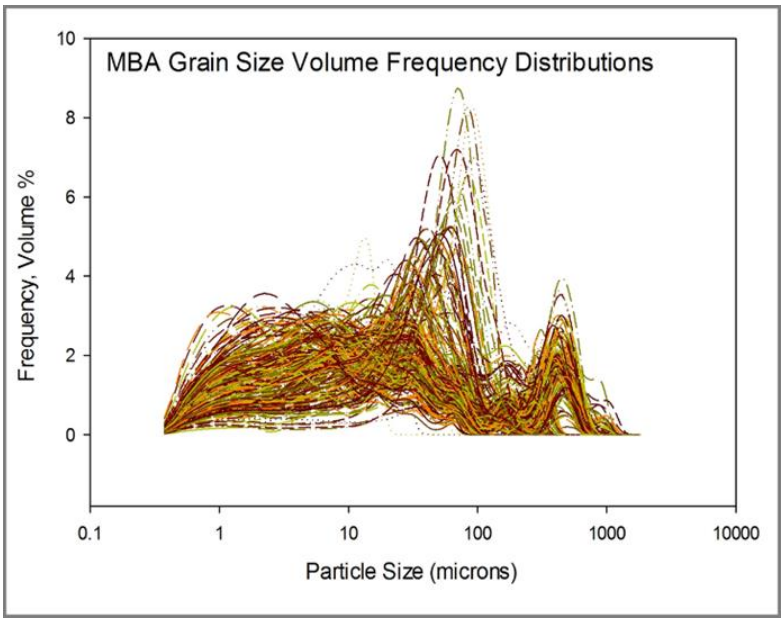

Figure 5. The grain size volume frequency distribution has three modes, at ~5 microns (clay-fine silt), ~62-100 microns (fine-very fine sand), and ~400-500 microns (medium sand). Coarse fraction likely represents shell debris.

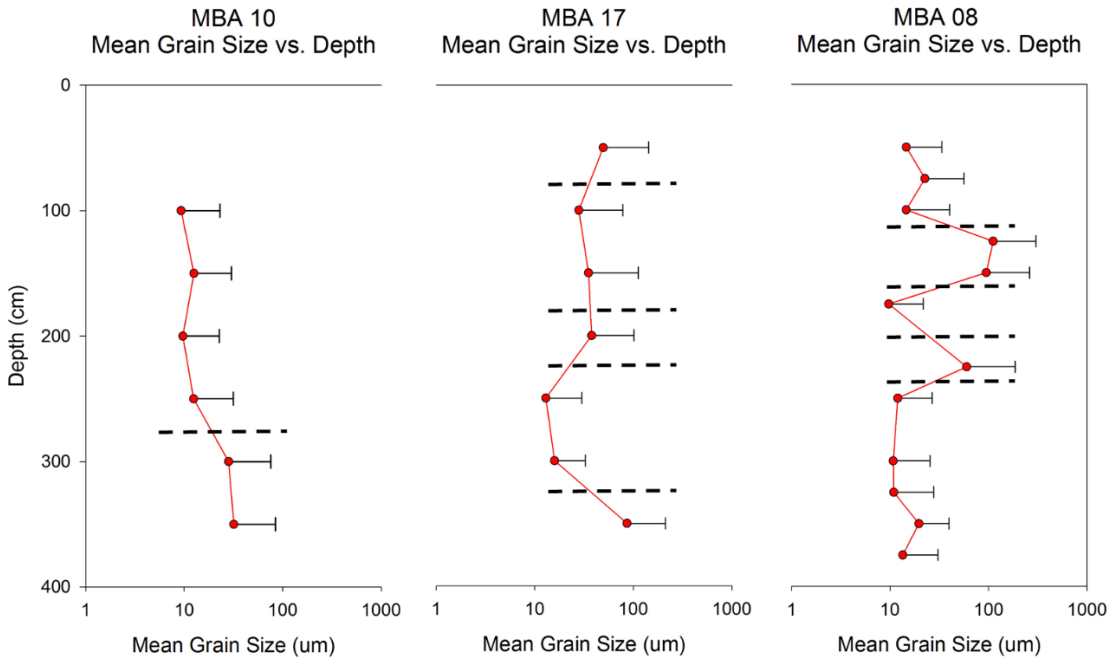

Figure 6. Representative mean grain size at depth, taken from sediment cores MBA 08, MBA 17, and MBA 10. A transition in grain size modes are denoted by dashed lines. Samples were taken at either 25 or 50 cm intervals. These transitions can be correlated to the change in bulk densities seen in Figure 4. The lower resolution of the grain size data means it is less capable of identifying these transitions, however, resulting in the fewer transitions seen here.

Grain size analysis results show consistent trends throughout the basin, generally consisting of a fining upwards profile, such as MBA 10 in Figure 6. However, it is not entirely uncommon to observe a series of fining progressing to coarsening upward in the profiles, sometimes followed by another trend of upwards fining, and terminated by coarse spike at the near-surface (Figure 6, MBA 17). This coarse spike is not always observed, but this is likely due to the relatively low spatial resolution of 25-50 cm intervals (Figure 6, MBA 08 and MBA 10). Furthermore, a few cores demonstrate a cycle between fining and coarsening upwards (Figure 6, MBA 08). The thickness of the near-surface coarse unit, while present across the basin, is widely variable, as is any underlying units with a different grain size transitional pattern.

3.3. Loss-on-Ignition

Loss-on-ignition results have clearly identified trends of organic content throughout the basin (Figure 7). Most highly organic sediments are present at depths between 0-1 m, sometimes exceeding 80% organic content. Additionally, a cloud of samples with high organic content is apparent at depths between ~2-2.5 m in several of the cores, and reach fractions as high as 82%. The pre-dried weights of the samples also inform on the fluid content of the material, with the fluid rich surface sediment possessing up to ~80% hydration (relative to both minerals and organics).

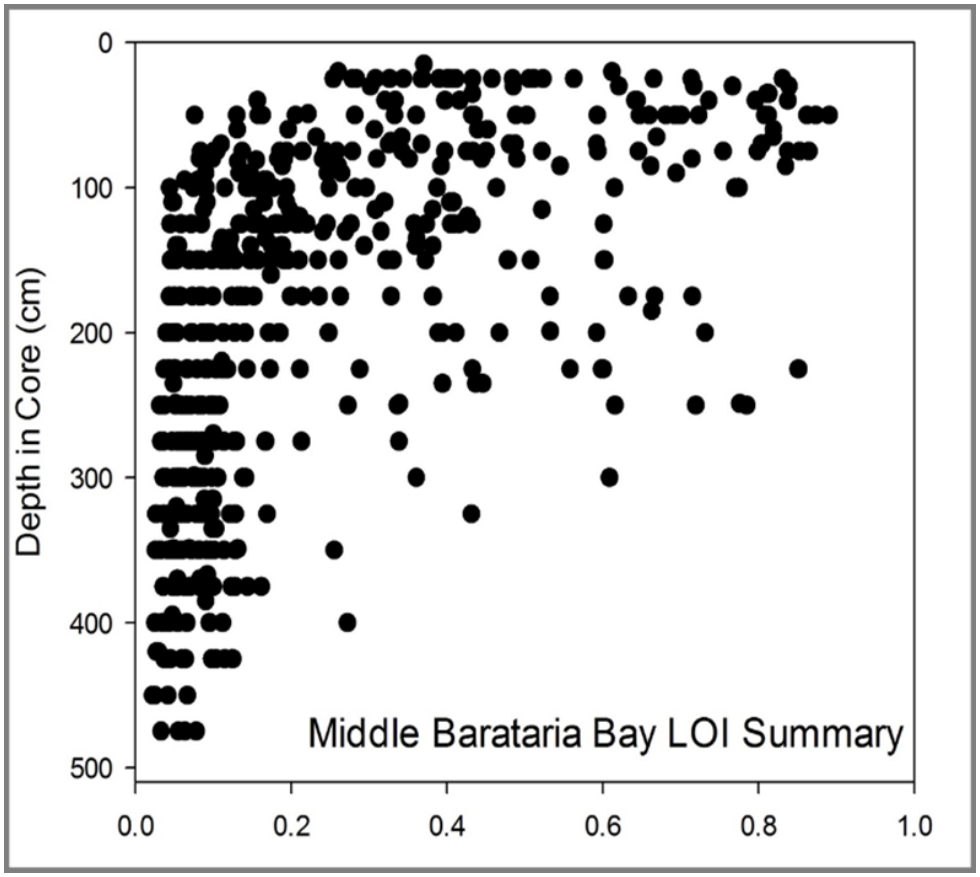

Figure 7. LOI results for the MBA study area. Organic concentrations exist at the surface and at depth (~200-250 cm).

Figure 8 contains representative profiles that both identify the decreasing organic content downcore from the near-surface, and the presence of organic-rich material at depth (MBA 08 and MBA 17). These organic-rich phases are correlative to the increased grain size means and diminished bulk density values observed in the previous results (Figures 4-6).

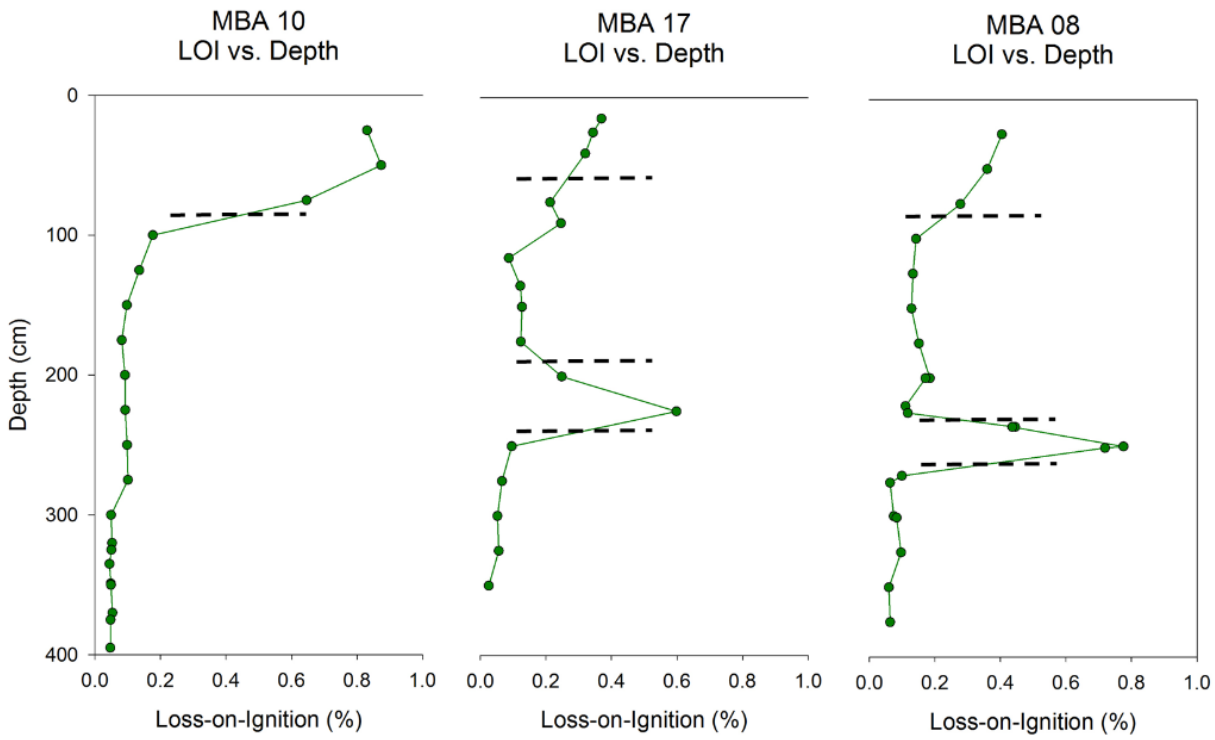

Figure 8. Representative organic content fraction at depth profiles, taken from MBA 08, MBA 17, and MBA 10. Transitions in high organic content lithology occurs at the near-surface (~50-80 cm) in each of the cores. A high organic fraction is recurrent at depth in MBA 08 and MBA 17 (~200-250 cm). These organic-rich intervals show up in Figure 4 as bulk density lows and Figure 6 as subdued spikes in mean grain size.

3.4. Lithology

The high resolution imagery demonstrates three separate lithologic trends (Figure 9). These lithologies are identified by the observation and inspection of the sediment, in addition to the physical properties determined through the previous tests.

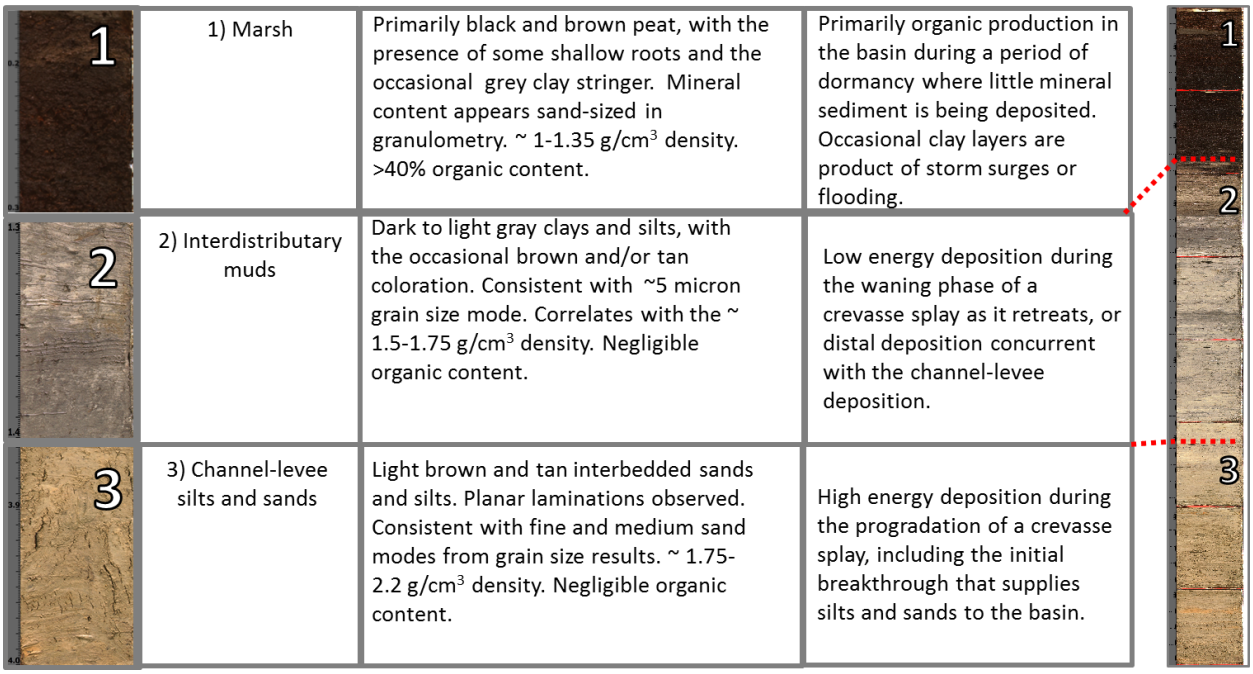

Figure 9. Observed lithology. The three observed distinct lithologies can be correlated to the density, grain size, and organic content properties (Figures 4-8). Full scan of core MBA 10 demonstrates a lithologic succession of the different lithologies, transitioning downcore from organic-rich peats, to grey silty muds, to interbedded sands and silts.

The lithology consistent with low density (~1-1.35 g/cm^3) and high organic fractions (>40%) is an organic-rich peat, present at the surface of every sediment core, and occasionally appearing at depth. It has a black and dark brown coloration, with the presence of roots in the shallow subsurface, and grey clay stringers interspersed throughout the basin. An isopach map of the surficial peat lithology (Figure 10) demonstrating that the base of the unit is undulatory, apparently filling a shallow trough that inclines downward gently from the southeast to northwest.

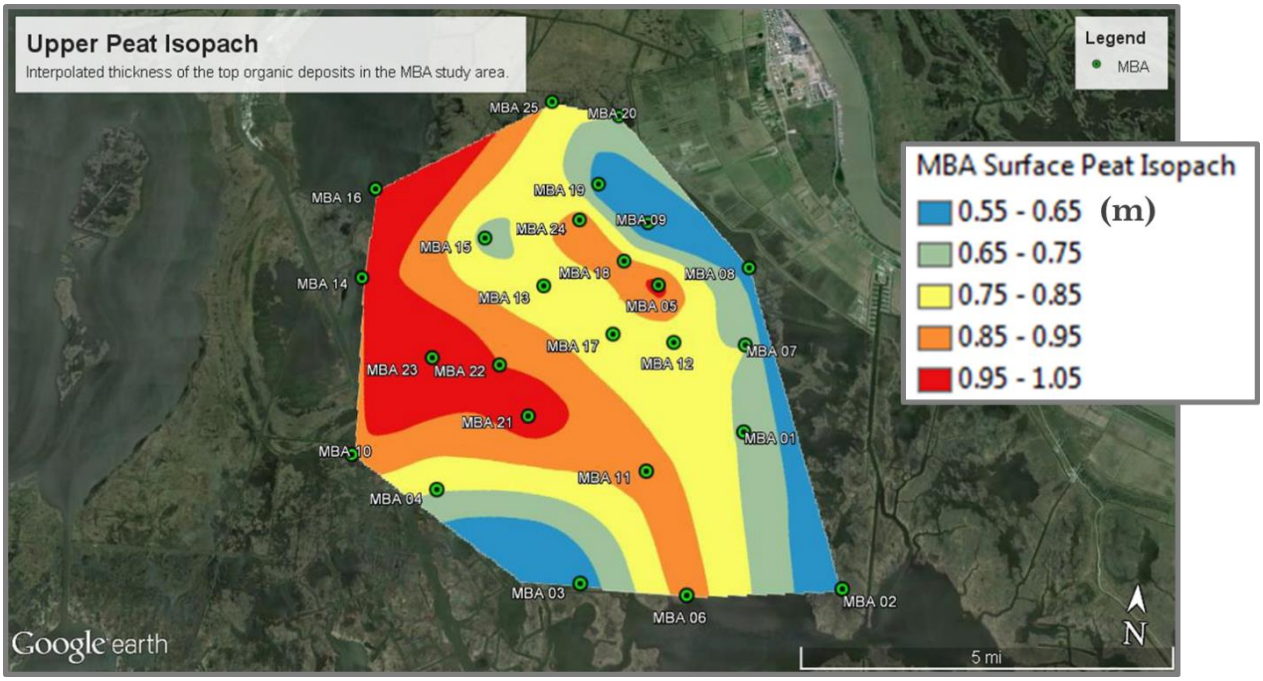

Figure 10. Isopach map of the study area depicting the change in thickness of the surficial peat layer of the marsh. Of particular note is MBA 17, with the lowest identified whole core sedimentation rate, which lies in a region of relative thin thickness. This could identify a zone that resisted regional subsidence. Alternatively, the surrounding areas could be examples of paleochannel fill.

The clay and silt-sized granulometry mode correlates to grey silty muds, typically following in the sequence. The dark to light grey coloration is generally consistent, though it is occasionally seen in tan and brown variants. The moderate density values (~1.5-1.75 g/cm^3) with low organic fractions are indicative of this material.

The final lithologic trend is an interbedded sand and silt layer that tends to end the sequence downcore. With a light brown and tan coloration, it is indicative of the fine and medium sand-sized mode discovered in the grain size experiments. It has a low organic content, observable planar laminations, and a greater density than the other lithologies (~1.75-2.2 g/cm^3.)

Although the different lithologies typically appear in this sequence, some sediment cores observe the sequence being recursive (MBA 08 in Figures 4 and 6), while others are absent certain layers. In a few of the cores, both of these situations occur at the same time. However, these lithologies have the same characteristics basin-wide.

3.5. Geochronology

The ^{137}Cs activity results demonstrate a peaks of activity at 48 cm, 50 cm, and 42 cm for cores MBA 08, MBA 22 and MBA 10 (respectively, Figure 11). Sedimentation rates calculated using this information and Equation 1 produce results of 0.92 cm/yr for MBA 08, 0.96 cm/yr for MBA 22, and 0.81 cm/yr for MBA 10.

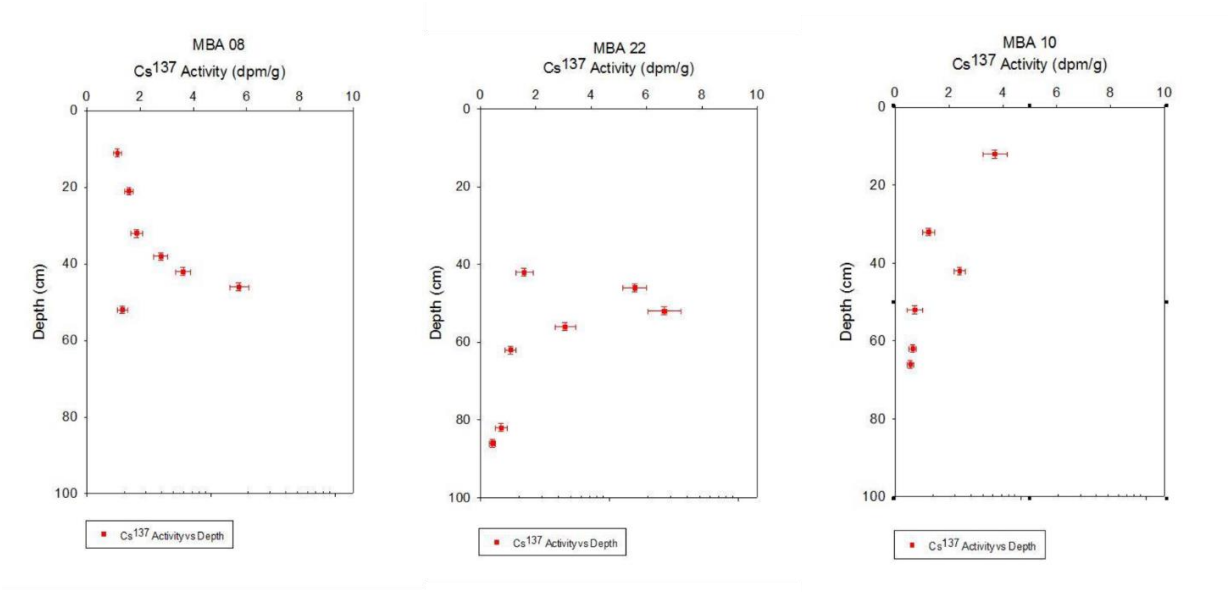

Figure 11. Cesium-137 results for MBA 08, 22, and 10. These values were used to calculate short-term sediment accumulation rates.

Finally, ten viable radiocarbon dating samples were completely processed (Table 2). Three types of samples were taken, each classified by the relative location of sampling in the core: base of surficial peat, top of subjacent peat at depth, and bottom of subjacent peat at depth. In addition, two bulk sediment samples were taken from clay-rich layers. However, the dates taken from these bulk-sediment samples are not included in the analysis because the early Holocene dates suggest that the organic carbon that was measured was allochthonous.

Table 2. Results of radiocarbon dating, including interval depth, type of sample, and both pre- and post-calibrated ages (INTCAL13 was the database used for calibration).

Core #	Interval (cm)	Description	Results (pre-Calibration)	Results (cal BP)	±
MBA 05	276-278	Base of Subjacent Peat	2350	2350	30
MBA 08	40-42	Base of Surface Peat	205	280	30
MBA 08	229-230	Top of Subjacent Peat	1965	1910	30
MBA 08	267-269	Base of Subjacent Peat	2685	2770	30
MBA 08	315-317	Bulk Sediment (Clay)	9105	10240	30
MBA 10	93-95	Base of Surface Peat	1010	870	30
MBA 11	215-217	Base of Subjacent Peat	2330	2340	30
MBA 13	289-291	Base of Subjacent Peat	2440	2610	30
MBA 16	374-376	Bulk Sediment (Clay)	11310	13140	30
MBA 17	72-74	Base of Surface Peat	340	550	30
MBA 17	213-215	Base of Subjacent Peat	2330	2270	30
MBA 22	163-165	Base of Subjacent Peat	2190	2130	30

Base of peat ages ranged between 280 and 870 ± 30 years ^{14}C years B.P. (before present, where present is 1950 A.D.), with the age increasing in conjunction with distance from the present day river channel (MBA 08 at 40-42 cm, MBA 17 at 72-74 cm, and MBA 10 at 93-95 cm, locations shown on Figure 3). The base of subjacent peat at depth ranges between 2130 and 2770 ± 30 ^{14}C years B.P., a slightly more constrained range that has a marginal decreasing trend further from the main river channel (MBA 08 at 267-269 cm, MBA 05 at 276-278 cm, MBA 17 at 213-215 cm, and MBA 22 at 163-165 cm, locations shown on Figure 3). Finally, the top of subjacent peat in MBA 08 was

measured at an age of 1910 ± 30 ^{14}C years B.P. Taking into an account the base of subjacent peat age (2770 ± 30 ^{14}C years B.P.), the subjacent peat layer in MBA 08 represents a minimum age duration of 860 ± 30 ^{14}C years B.P.

Additionally, the approximate whole core sedimentation rate of MBA 08 is calculated at ~1 mm/yr according to the base of subjacent peat's ^{14}C date at 2.67 m (2770 +/- 30 years B.P.) Additional calculated whole core sedimentation rates vary within a 0.9 to 1.2 mm/yr range, with the exception of MBA 17, with an approximate rate of 0.7 mm/yr, which correlates with a relatively thinner surficial peat layer (Figure 10).

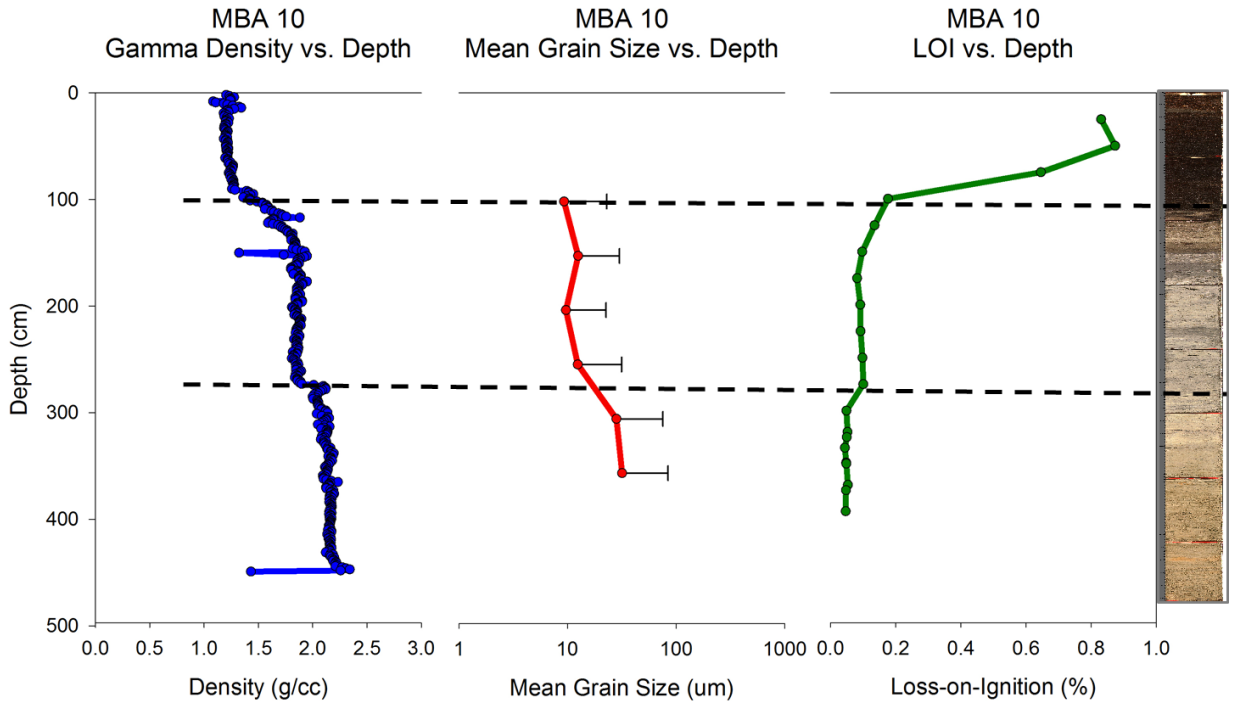

Figure 12. The regressive subdelta lithofacies succession, as seen in sediment core MBA 10. The transition from the Channel-Levee Silts and Sands high energy environment (sand and silt size interbedded grains, ~1.75-2.2 g/cc bulk density, near-zero organic percentage), to the Interdistributary Muds low energy environment (silty muds with low organic percentage and ~1.5-1.75 g/cc), and to the Marsh dormant environment (>40% organic percentage and ~1-1.35 g/cc bulk density) is demonstrated in both the high resolution imagery and the recorded physical properties.

Chapter 4. Discussion

4.1. Facies Model

A subdelta's lithofacies reflect its growth and decline. Mineral sediment supply first increases as incipient channels enlarge, then declines due to hydraulic inefficiency, and mineral supply is replaced by organic production (Coleman and Gagliano, 1964). Thus, any evidence of subdelta evolution will reflect this cycle of high energy deposition evolving into a low energy or dormant condition. Our results demonstrate substantial vertical and lateral variability that nevertheless generally conform to a subdelta model (Coleman and Gagliano, 1964).

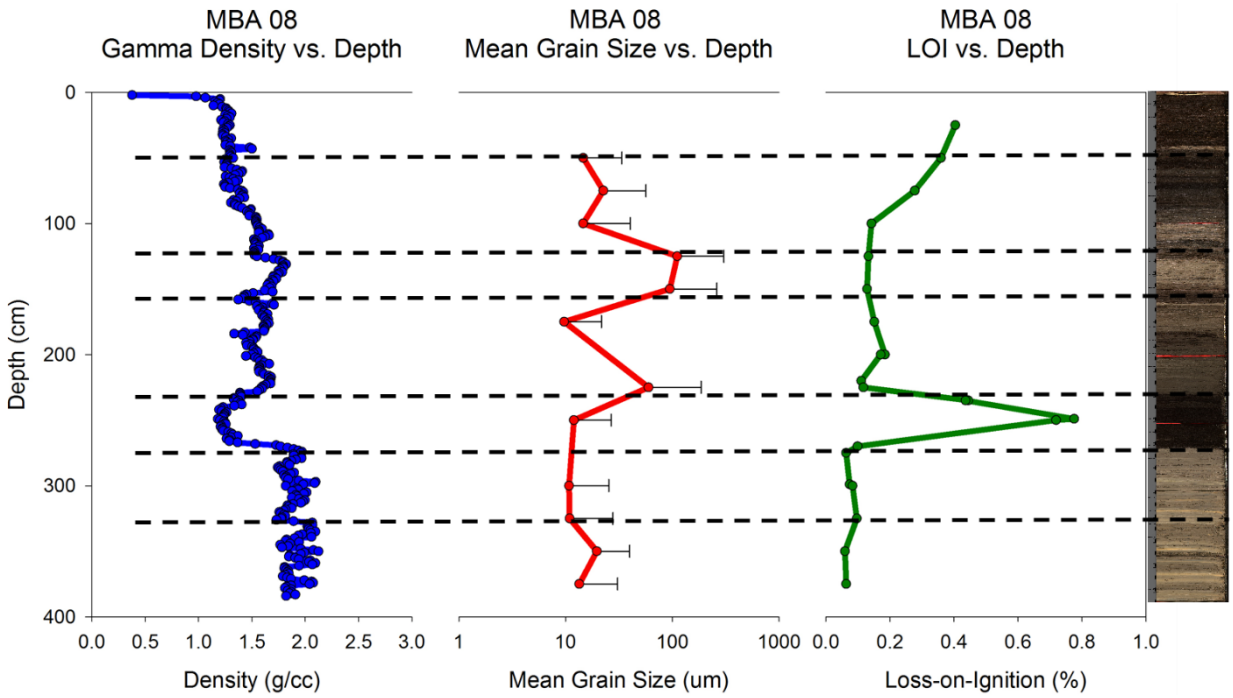

Figure 13. A cyclical subdelta lithofacies succession, as seen in sediment core MBA 08. While it shares the Channel-Levee Silts and Sands / Interdistributary Muds / Marsh transition as seen in MBA 10, the Marsh dormancy period then transitions back into a low energy Interdistributary Muds phase, followed by a return to the Channel-Levee Silts and Sands facies. The facies then exhibit the expected succession back through Interdistributary Muds and Marsh dormancy at the near-surface. Thus, this facies succession suggests at least two separate subdelta events.

The lithology discovered in the sediment cores corresponds to a three phase succession of lithofacies (Figures 9, 12 and 13). The high energy phase of deposition represents initial breakthrough of a crevasse splay, a major land building event that is responsible for the transport of sand and silt size grains into the basin, referred to herein as channel-levee silts and sands. The parameters for this facies can be derived from measured physical properties and observed traits. This lithofacies is typically of brown or tan coloration, has interbedded sands (fine to medium-grained) and silts (the two coarser particle-sized modes in Figure 5), has a bulk density of approximately 1.75 to 2.2 g/cm^3 (such as the deepest point of all three cores in Figure 4,) and has a near-zero organic fraction (a feature seen in the deepest portion of MBA 10 in Figure 8).

The low energy phase of distal deposition as the crevasse splay wanes and retreats, referred to herein as the interdistributary muds lithofacies (Figure 12). Composed of dark grey silty muds (the ~5 micron mode in Figure 5), within a bulk density range of 1.5 – 1.75 g/cm^3 (observable in the three cores in Figure 4), the interdistributary muds lithofacies also has a very low organic fraction (observable in the middle phase of MBA 10 in Figure 8).

The marsh facies develops during the period of lowest mineral sediment supply, when sediment production is dominated by organic growth that produces highly organic, dark-colored peats. The marsh facies has an organic percentage that varies between 50-80% (seen basin-wide in Figure 7, at the near-surface in MBA 08, 17, and 10 in Figure 8, and at depth in MBA 08 and 17 in the same figure,) and the limited mineral

content appears sand-size when seen in grain size analysis (seen at the near-surface in Figure 6 in MBA 17). The bulk density is within a 1-1.35 g/cm^3 range (near-surface values in Figure 4, also recurring at depth in MBA 08 and 17,) with observable roots and clay stringers. These thin clay layers may reflect either energetic river flooding that temporarily reactivates dormant channels or storm-sediment deposition from the seaward direction in the basin, during a phase of mineral-sediment starvation typical of this phase of development.

Generally, these lithofacies are stacked in the upwards order of 1-2-3, producing an overall grain-size trend of fining upwards (MBA 10 in Figure 4), with some exceptions discussed in the next paragraph. Additionally, the transition between periods of coarsening upwards and fining upwards in some cores suggests a series of events, rather than a continuum (seen in MBA 08 and 17, Figure 6). This sequence, when combined with the modes present in the volume frequency distribution (Figure 5), is strong evidence for the lithofacies transitions of an aging crevasse-splay. While the silts and sands act as evidence of interspersed channel and levee deposition, the clays could represent the interdistributary period of regressing depositional activity.

Loss-on-ignition testing has identified both the concentrated organic sediment production of a dormant basin in the shallow subsurface (~0.1-1.2 m thick), and a similar period of organic-dominated sediment production at depth (~2-2.5 m below surface) in several of the cores (illustrated both in Figure 7 and in cores MBA 08 and 17 in Figure 8). This stacking pattern suggests multiple subdeltaic cycles in the basin, with the peat at depth indicating a period of dormancy that followed a crevasse-splay from an older

delta lobe. Additionally, the high organic fraction suggests that the Middle Barataria Receiving Basin has been deprived of mineral sedimentation in recent decades, with the high relative water and organic contents representative of the "drowning" effect of a subsiding basin. Combining the granulometry, gamma density, and organic fraction results provide the framework for a stratigraphic analysis, which suggest a deepening of strata away from the primary trunk of the river (Figures 14 and 15).

4.2. Interpreted Deltaic History

Stratigraphic cross sections (Figure 14) display characteristics of splay deposition. Radiocarbon dating results of 280 to 870 ± 30 ^{14}C years B.P. at the base of surficial peat can be used as a time estimate for the point of cessation of active mineral-sediment deposition in the basin. Thus, the uppermost lithofacies series can be associated with a subdelta during the Plaquemines-Belize delta-building cycle, which Tornqvist et al. (1996) have dated to have begun ca. 1322 ± 22 ^{14}C years B.P. and remains ongoing. The fining-upwards sequence present in the near-surface portion of every core is consistent with the hypothesis that this succession corresponds to Plaquemines-Belize progradation, deposited during the construction of the latest delta at its present location at the Mississippi Bird's Foot Delta. Chronologically the most recent splay, its regression towards the trunk channel created the age disparity in organic production of marsh peat relative to distance.

Furthermore, stratigraphic correlation of the buried peat facies and the recorded base of subjacent peat ages (2130 to 2770 ± 30 ^{14}C years B.P.) is evidence of a prior crevasse-splay cycle (or even a prior subdelta) tied to either the St. Bernard paleo

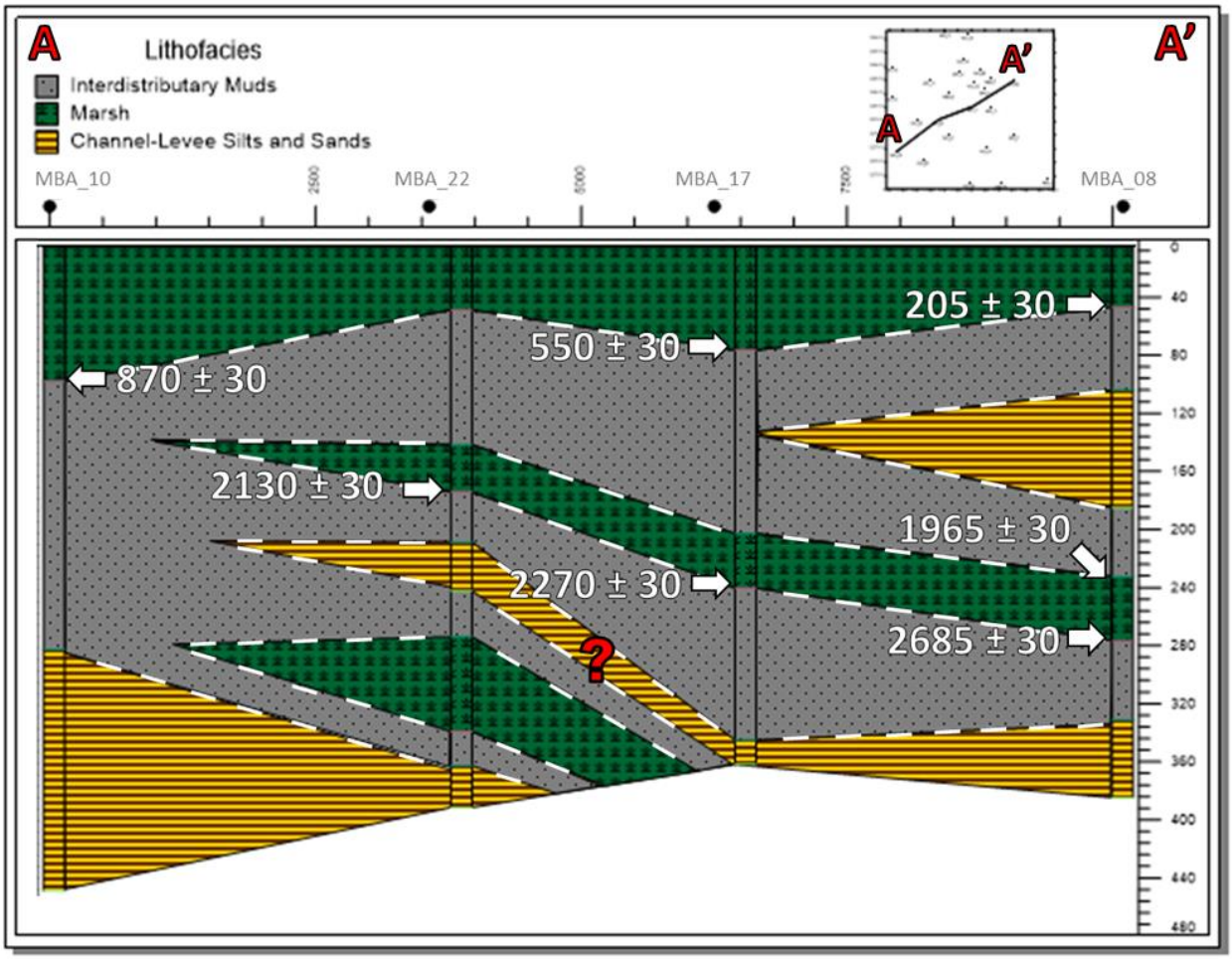

Figure 14. West-east stratigraphic cross section of MBA 08-17-22-10. Radiocarbon calibrated dates (BP) have been included at their appropriate location and depths. Cyclical facies succession implies up to two additional subdelta events preceding the current environment. Red question marks indicates questionable continuity.

delta lobe, or the LaFourche paleo delta lobe, dated to have their beginnings in ca. 3569 ± 24 and 1491 ± 13 ^{14}C years B.P. (respectively) by Tornqvist et al. (1996). The slight age disparity (with younger peat lying further west) and distribution (thickening towards the west) supports the LaFourche sourcing, while the timing is much more consistent with the St. Bernard. The discrepancies could be possibly be accounted for – the age and thickness distribution could be a product of the splay coming from a location further

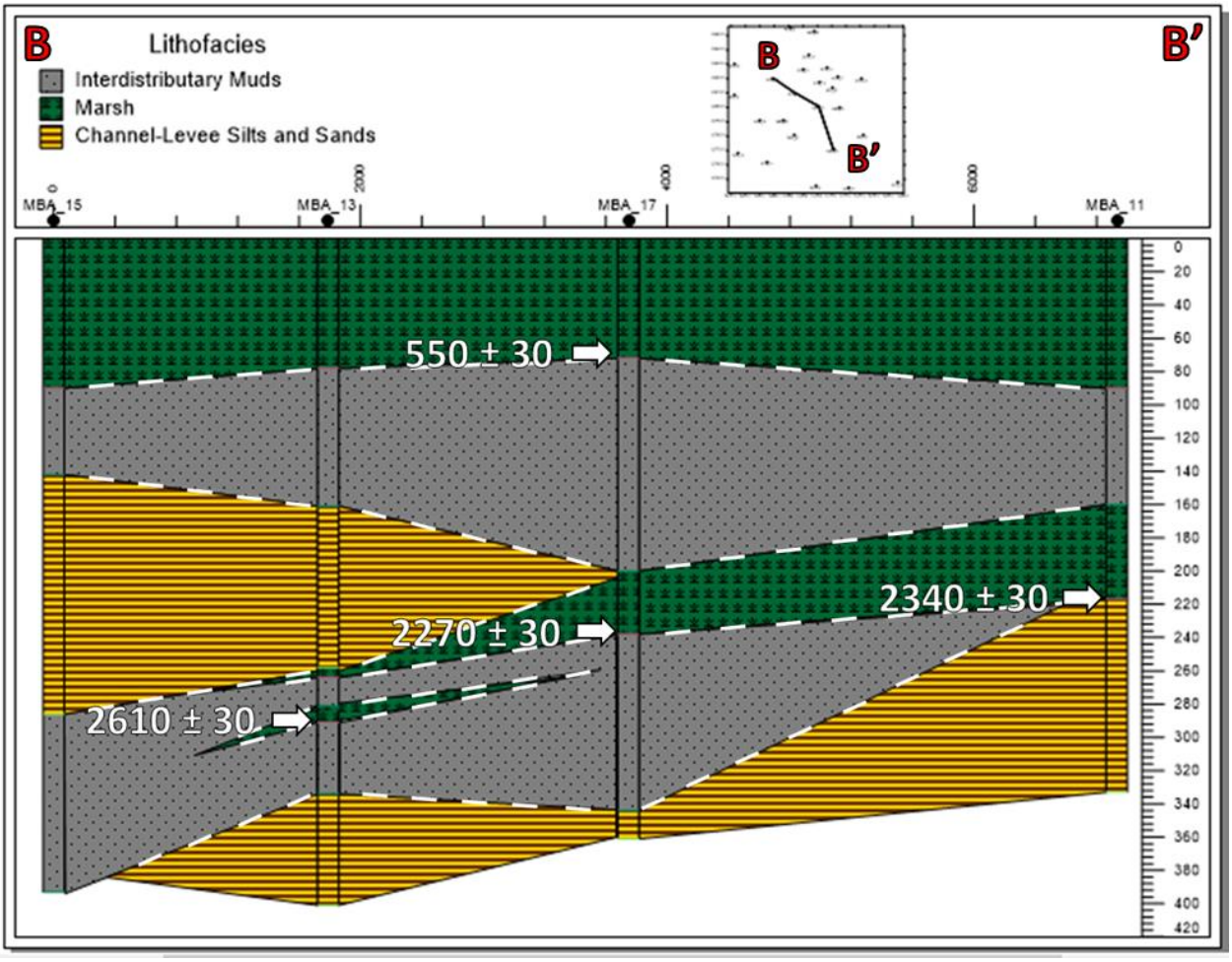

Figure 15. North-south stratigraphic cross section of MBA 15-13-17-11. Radiocarbon calibrated dates (BP) have been included at their appropriate location and depths. Due to the lack of clear lithofacies succession, the cross-section likely represents a stratigraphic view perpendicular to the principal movement of the basin subdelta record. Overlapping incongruent lithofacies suggest a combination of differential erosion and two separate subdelta events distinguished by different east-west vectors of propagation.

north, not the east as may be initially expected. Either way, radiocarbon dating suggests an organic production duration of 860 ± 30 ^{14}C years B.P. between this older event and the more recent Plaquemines-Belize event. Marshland scour could have removed organic deposition however, so this age must be treated both as a gross approximation and a minimum duration.

After identifying the most recent splay lithofacies succession that exists in the cores, and correlating the base of interdistributary deposition (when possible), an isopach could be developed for the stratigraphic distribution of the event in the sedimentary record (Figure 16). The thickening of the succession away from the trunk channel demonstrates the extent of the flooding during the event, while possibly infilling channels and zones of subsidence from previous events. It could also indicate that the source of the crevasse splay was located further north of the study area. The presence of this older, consolidated sediment depth could be good evidence that there is low compressibility and subsidence at depths greater than 2-3 m in the basin.

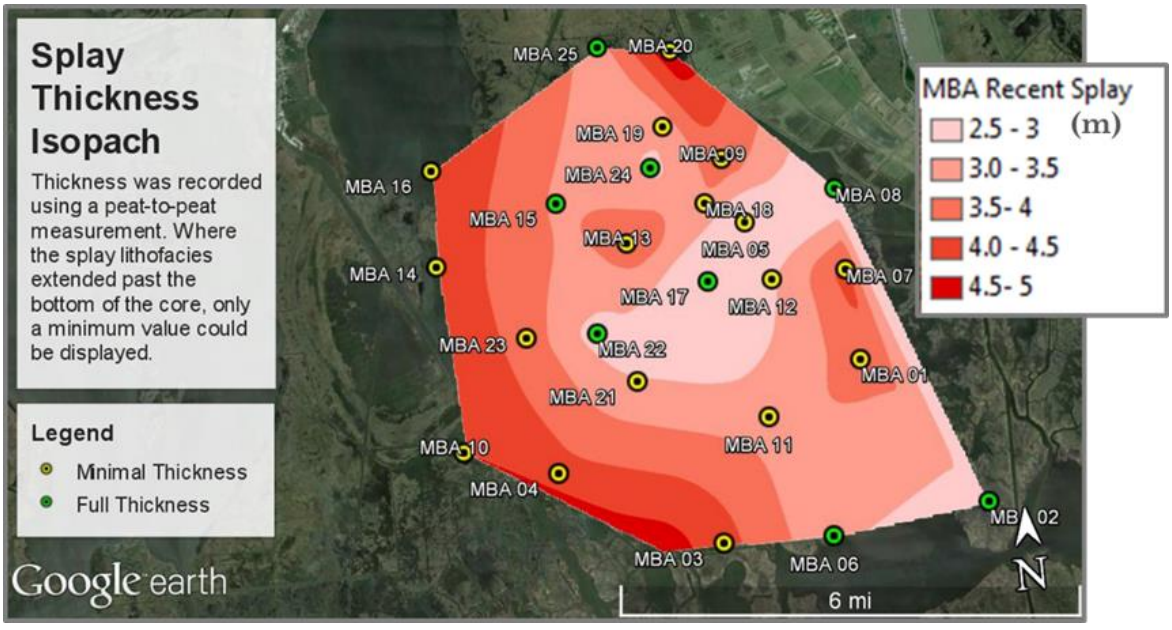

Figure 16. Thickness distribution for the crevasse-splay lithofacies. It is expected that this represents an event during the Plaquemines-Belize delta progradation, has been measured via top of peat to top of peat at depth. It should be noted not all cores had peat at depth to constrain the lithofacies succession, and thus represent a minimum thickness.

The buried peat of the previous splay cycle was likely produced from a crevasse splay event from Bayou Barataria. The stream courses of the bayou identified by the work of Fisk, 1944 are consistent with the study area and provide a credible St. Bernard era sourcing (Figure 17). The particularly thin layer of Marsh peats seen in Figure 15 are indicative the kind of scour the basin experienced, possibly due to crevasse splay events that did not develop into subdelta building.

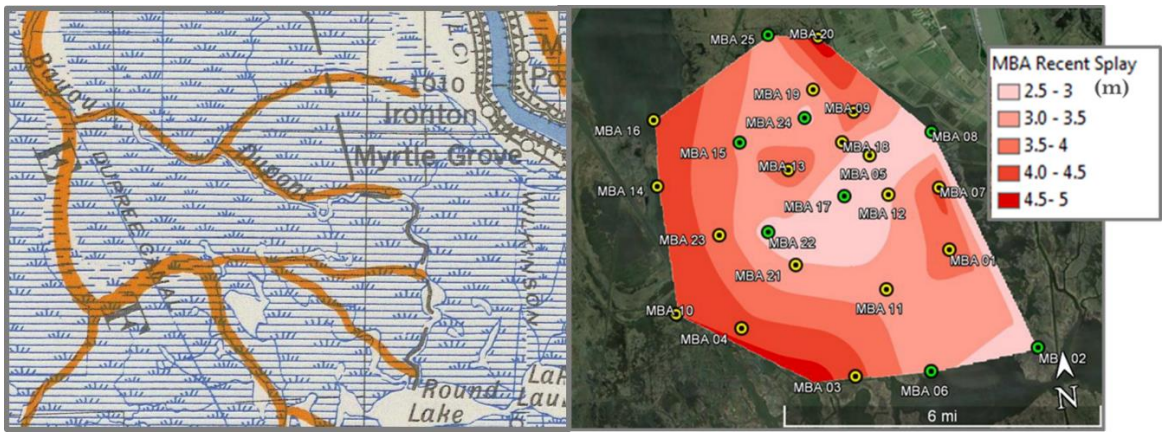

Figure 17. Mapped Bayou Barataria stream courses of the Mississippi alluvial valley (left) taken from Fisk, 1944. On the right is the splay isopach produced by this study. These streams provide a feasible origin for the splay material at depth in the study area.

4.3. Implications for Sediment Diversions

Results of this study have some implications for land-building associated with the proposed Middle Barataria Diversion (LACPRA, 2012). The radiocarbon dated sediments from across the basin can be used to constrain a relative sea level rise (including the subsidence factor) over a time period of 1000-3000 years, a rate in the range of ~0.1-0.33 cm/y. Short-term RSLR, calculated using the ^{137}Cs data, is in the range of ~0.54-0.69 cm/y. These results suggest that sediments near the depth of ^{14}C measurements are

subsiding more slowly than is the zone containing detectable ^{137}Cs. This can be explained by the most rapid subsidence occurring within peat-rich surface sediments.

The tendency of these sediments to compact (and allow the surface to subside) is likely a function of water content (e.g., Lo et al., 2015). The marsh and interdistributary muds facies have the highest water contents among the three lithofacies present, and so might be the most likely to compact and deform under loading induced by diversion-sediment deposition. Furthermore the marsh peats may be very susceptible to scour and erosion (e.g., Wilson and Allison, 2008), and may not hold up well to the discharge any sediment diversion would bring to the basin.

The channel-levee silts and sands have lower water content/porosity than the other two lithofacies, and so may be less likely to compact or deform under loading. However, the non-cohesive nature of these sand-rich sediments may also make them easily erodible (compared to consolidated muds) if exposed to energetic diverted flows.

Thus, while the upper 1-2 m of sediment is a risk for deformation upon the re-introduction of mineral nourishment, the sands present 2 m below surface may tolerate more loading without deformation. This resilience is further reinforced by the fact that sediments from the St. Bernard period of deposition have survived at relatively shallow depths (as shallow as ~1.3 m in MBA 22, as seen in Figure 14.) This fact, along with the presence of the consolidated channel-levee silts and sands, suggests lower subsidence and compressibility factors at depth, particularly below 2 m. Therefore while the bay has a fast RSLR, there is sufficient evidence that with significant mineral sediment contribution it could resist further deterioration due to a resilient foundation at depth.

Chapter 5. Conclusions

The stratigraphic layout and physical properties of the sediments of Middle Barataria Bay support a subdelta model with multiple recurrences in the last ~3000 years. The identified lithofacies for these subdelta events have distinct physical parameters, generally follow a consistent pattern in the sediment record, and represent a transition from high energy deposition (Channel-Levee Silts and Sands), to low energy distal deposition (Interdistributary Muds), to an organic production dominated period of dormancy (Marsh). This succession is analogous to the crevasse splay model of deposition that forms the foundation of subdelta cycles. Stratigraphic correlation suggests propagation trending perpendicular to the present-day trunk channel, with separate cycles occurring further north-south of each other instead of directly along the paths of previous events.

The radiocarbon dating results of 280 to 870 ± 30 ^{14}C years B.P. taken from the base of peat in the surficial Marsh facies presents the cessation of active mineral-sediment deposition in the basin, suggesting the uppermost lithofacies series is associated with a subdelta during the Plaquemines-Belize delta-building cycle, an ongoing delta lobe dated to have begun ca. 1322 ± 22 ^{14}C years B.P. (Tornqvist et al., 1996). The buried Marsh facies (evidence of previous subdelta cycles) was dated to have begun deposition within a range of 2130 to 2770 ± 30 ^{14}C years B.P., attributing the event(s) to either the LaFourche or St. Bernard delta lobes. While stratigraphic analysis leans towards the former, the St. Bernard is favored as the source due to a much closer correlation with the dates put forth by Tornqvist et al. (1996). Furthermore, the period

of mineral sediment starvation in the basin between the cessation of St. Bernard activity and the commencement of Plaquemines-Belize deposition is dated to have a minimum duration of 860 ± 30 ^{14}C years B.P.

The basin's stratigraphy and deltaic history are promising for the projected success of sediment diversion projects in the region. While the near-surface lithofacies are susceptible to erosion and compaction, the presence of channel sands suggests a firm foundation resistant to compression. Furthermore, the survival of St. Bernard sourced sediments in the relative near-surface suggests resilience to compaction and subsidence at depths greater than 2 m. These factors, when taken into account with the dangers of a high RSLR in the area (~0.54-0.69 cm/y), suggest that Middle Barataria Bay could provide a stable foundation for mineral sediment nourishment while also providing one of the greater possible impacts of active land-building efforts along the Mississippi River Delta.

References

Allison, M. A., & Meselhe, E. A. (2010). The use of large water and sediment diversions in the lower Mississippi River (Louisiana) for coastal restoration. Journal of Hydrology, 387(3), 346-360.

Bentley, S. J., Blum, M. D., Maloney, J., Pond, L., & Paulsell, R. (2015). The Mississippi River source-to-sink system: Perspectives on tectonic, climatic, and anthropogenic influences, Miocene to Anthropocene. Earth-Science Reviews, 153, 139-174.

Blum, M. D., & Roberts, H. H. (2012). The Mississippi delta region: past, present, and future. Annual Review of Earth and Planetary Sciences, 40, 655-683.

Bridge, J. S. (1984). Large-scale facies sequences in alluvial overbank environments. Journal of Sedimentary Research, 54(2), 583-588.

Coleman, J. M., & Gagliano, S. M. (1964). Cyclic sedimentation in the Mississippi River deltaic plain. Gulf Coast Association of Geological Societies Transactions, 14, 67-80.

Coleman, J. M. (1988). Dynamic changes and processes in the Mississippi River delta. Geological Society of America Bulletin, 100(7), 999-1015.

Davis DW (2000) Historical perspective on crevasses, levees, and the Mississippi River, pp 84–106. In: Colten CE (ed) Transforming New Orleans and its environs, University of Pittsburgh Press, Pittsburgh, pp 272

Elliott, T. (1974). Interdistributary bay sequences and their genesis. Sedimentology, 21(4), 611-622.

Fitzgerald, D., Kulp, M., Hughes, Z., Georgiou, I., Miner, M., Penland, S., & Howes, N. (2007). Impacts of rising sea level to backbarrier wetlands, tidal inlets, and barrier islands: Barataria Coast, Louisiana. In Proc Coastal Sediments, 7, 1179-1192.

Fitzgerald, D. M., Kulp, M., Penland, S., Flocks, J., & Kindinger, J. (2004). Morphologic and stratigraphic evolution of muddy ebb-tidal deltas along a subsiding coast: Barataria Bay, Mississippi River Delta. Sedimentology, 51(6), 1157-1178.

Fisk, H. N. (1944). Geological investigation of the alluvial valley of the lower Mississippi River (p. 78). War Department, Corps of Engineers.

Heiri, O., Lotter, A. F., & Lemcke, G. (2001). Loss on ignition as a method for estimating organic and carbonate content in sediments: reproducibility and comparability of results. Journal of paleolimnology, 25(1), 101-110.

LACPRA (Louisiana Coastal Protection and Restoration Authority), 2012, Louisiana's Coastal Master Plan. Online at http://www.coastalmasterplan.louisiana.gov/

Nittrouer, C. A., DeMaster, D. J., Mckee, B. A., Cutshall, N. H., & Larsen, I. L. (1983). The effect of sediment mixing on Pb-210 accumulation rates for the Washington continental shelf. Marine Geology, 54(3), 201-221.

Paola, C., Twilley, R. R., Edmonds, D. A., Kim, W., Mohrig, D., Parker, G., Viparelli, E., & Voller, V. R. (2011). Natural processes in delta restoration: Application to the Mississippi Delta. Annual Review of Marine Science, 3, 67-91.

Reimer, P. J., Bard, E., Bayliss, A., Beck, J. W., Blackwell, P. G., Ramsey, C. B., Buck, C. E., Cheng, H., Edwards, R. L., Friedrich, M., Grootes, P. M., Guilderson, T. P., Haflidason, H., Hajdas, I., Hatte, C., Heaton, T. J., Hoffmann, D. L., Hogg, A. G., Hughen, K. A., Kaiser, K. F., Kromer, B., Manning, S. W., Niu, M., Reimer, R. W., Richards, D. A., Scott, E. M., Southon, J. R., Staff, R. A., Turney, C. S. M., & van der Plicht, J. (2013). IntCal13 and Marine13 radiocarbon age calibration curves 0-50,000 years cal BP. Radiocarbon, 55, 1869-1867.

Roberts, H. H. (1997). Dynamic changes of the Holocene Mississippi River delta plain: the delta cycle. Journal of Coastal Research, 13(3), 605-627.

Sasser, C. E., Dozier, M. D., Gosselink, J. G., & Hill, J. M. (1986). Spatial and temporal changes in Louisiana's Barataria Basin marshes, 1945–1980. Environmental Management, 10(5), 671-680.

Talma, A. S., & Vogel, J. C. (1993). A simplified approach to calibrating (super 14) C dates. Radiocarbon, 35(2), 317-322.

Tornqvist, T. E., Kidder, T. R., Autin, W. J., & van der Borg, K. (1996). A revised chronology for Mississippi River subdeltas. Science, 273(5282), 1693-1696.

Törnqvist, T. E., Wallace, D. J., Storms, J. E., Wallinga, J., Van Dam, R. L., Blaauw, M., Derksen, M. S., Klerks, C. J. W., Meijneken, C., & Snijders, E. M. (2008). Mississippi Delta subsidence primarily caused by compaction of Holocene strata. Nature Geoscience, 1(3), 173-176.

Wells, J. T., & Coleman, J. M. (1987). Wetland loss and the subdelta life cycle. *Estuarine, Coastal and Shelf Science*, *25*(1), 111-125.

Wilson, C. A., & Allison, M. A. (2008). An equilibrium profile model for retreating marsh shorelines in southeast Louisiana. Estuarine, Coastal and Shelf Science, 80(4), 483-494.

Wright, L. D., and C. A. Nittrouer. (1995). Dispersal of river sediments in coastal seas: six contrasting cases. Estuaries, 18(3), 494-508.

Xu, K., Bentley, S. J., Robichaux, P., Sha, X., & Yang, H. (2016). Implications of Texture and Erodibility for Sediment Retention in Receiving Basins of Coastal Louisiana Diversions. Water, 8(1), 26.

Vita

Joseph Ethan Thomas Hughes, a native of Tyler, Texas, received his bachelor's degree in Exploration Geology at Millsaps College in Jackson, Mississippi. This was followed by a period of employment with XRI Geophysics as a Project Geophysicist in Vicksburg, Mississippi, taking part in several of their ongoing projects. However, he soon returned to his plans for higher education and attended the graduate school in the Department of Geology and Geophysics at Louisiana State University. He is slated to receive his master's degree in December of 2016, and plans to enter the work force in the field of environmental science.